[redacted]

Copy 44
RM SL50B23

RESEARCH MEMORANDUM

for the

Air Materiel Command, U. S. Air Force

FREE-FLIGHT INVESTIGATION OF THE STATIC AND DYNAMIC LONGITUDINAL STABILITY CHARACTERISTICS OF $\frac{1}{3.7}$-SCALE ROCKET-POWERED MODELS OF THE BELL MX-776A

By David H. Michal

Langley Aeronautical Laboratory
Langley Air Force Base, Va.

NATIONAL ADVISORY COMMITTEE FOR AERONAUTICS

WASHINGTON

[redacted]

NACA RM SL50B23

NATIONAL ADVISORY COMMITTEE FOR AERONAUTICS

RESEARCH MEMORANDUM

for the

Air Materiel Command, U. S. Air Force

FREE-FLIGHT INVESTIGATION OF THE STATIC AND DYNAMIC LONGITUDINAL STABILITY CHARACTERISTICS OF $\frac{1}{3.7}$-SCALE ROCKET-POWERED MODELS OF THE BELL MX-776A

By David H. Michal

SUMMARY

An investigation of the static and dynamic longitudinal stability characteristics of $\frac{1}{3.7}$-scale rocket-powered models of the Bell MX-776A has been made for a Mach number range from 0.8 to 1.6. Two models were tested with all control surfaces at 0° deflection and centers of gravity located 1/4 and 1/2 body diameters, respectively, ahead of the equivalent design location. Both models were stable about the trim conditions but did not trim at 0° angle of attack because of slight constructional asymmetries.

The results indicated that the variation of lift and pitching moment was not linear with angle of attack. Both lift-curve slope and pitching-moment-curve slope were of the smallest magnitude near 0° angle of attack.

In general, an increase in angle of attack was accompanied by a rearward movement of the aerodynamic center as the rear wing moved out of the downwash from the forward surfaces. This characteristic was more pronounced in the transonic region.

The dynamic stability in the form of total damping factor varied with normal-force coefficient but was greatest for both models at a Mach number of approximately 1.25. The damping factor was greater at the lower trim normal-force coefficients except at a Mach number of 1.0. At that speed the damping factor was of about the same magnitude for both models.

The drag coefficient increased with trim normal-force coefficient and was largest in the transonic region.

INTRODUCTION

At the request of the Air Materiel Command, U. S. Air Force, the Pilotless Aircraft Research Division of the Langley Laboratory has conducted an investigation of the Bell MX-776 by means of rocket-propelled models flown at its testing station at Wallops Island, Va. As the preliminary investigation of the Bell MX-776B had shown the configuration to be longitudinally unstable at small angles of attack (reference 1), a more searching investigation of the longitudinal stability of the Bell MX-776A, a similar configuration with better stability characteristics, was deemed necessary. Two $\frac{1}{6}$-scale models of the Bell MX-776B were modified to simulate $\frac{1}{3.7}$-scale models of the Bell MX-776A and instrumented to measure angle of attack and normal acceleration.

The investigation of the longitudinal stability of the Bell MX-776A was accomplished by a technique which consisted of analyzing the time histories of angle of attack and normal acceleration as the model experienced short-period oscillations caused by vertical-thrusting pulse rockets during the decelerating portion of the flight. Since the angles of attack were small, normal force was considered lift. The investigation covered a Mach number range from 0.8 to 1.6.

SYMBOLS

M	Mach number
R	Reynolds number based on body diameter
V	flight-path velocity, feet per second
q	dynamic pressure, pounds per square foot $\left(\frac{\rho V^2}{2}\right)$
ρ	density, slugs per cubic foot
g	acceleration due to gravity, feet per second per second
W	weight of model, pounds

S_f	body frontal area (0.1758 sq ft)
d	body diameter (0.473 ft)
I_y	moment of inertia about pitch axis, slug-feet square
a_n	normal acceleration, feet per second per second
α	angle of attack, degrees
P	period of short-period oscillations, seconds
C_N	normal-force coefficient $\left(\frac{\text{Normal force}}{qS_f}\right)$
C_D	drag coefficient $\left(\frac{\text{Drag}}{qS_f}\right)$
C_{L_α}	rate of change of lift coefficient with angle of attack, per degree
C_{m_α}	rate of change of pitching-moment coefficient with angle of attack, per degree $\frac{d\left(\frac{M}{qS_f d}\right)}{d\alpha}$
$T_{1/2}$	time to damp to one-half amplitude, seconds
$C_{m_{\frac{\dot{\theta} d}{2V}}} + C_{m_{\frac{\dot{\alpha} d}{2V}}}$	total damping factor, per degree
$\dot{\alpha}$	rate of change of angle of attack with time, degrees per second $\left(\frac{d\alpha}{dt}\right)$
$\dot{\theta}$	rate of change of angle of pitch with time, degrees per second $\left(\frac{d\theta}{dt}\right)$

MODELS

The models used in the subject investigation were $\frac{1}{6}$-scale models of the Bell MX-776B as described in reference 1 modified to approximately simulate $\frac{1}{3.7}$-scale models of the Bell MX-776A. In order to approximate

[redacted]

the Bell MX-776A configuration it was necessary to extend the body center section 5 inches, to reduce the exposed area of the forward horizontal fins, and to increase the aspect ratio of the rear vertical fins. The modified models still differed from the Bell MX-776A in that the nose was of an elliptical cross section rather than a circular cross section, and the tail section was less tapered.

The same propulsion system was used as described in reference 1. Four vertical-thrusting pulse rockets were mounted under the surface of the fuselage just forward of the rear fin assembly. These rockets were delayed to fire individually during the decelerating portion of the flight.

Figure 1 shows a three-view drawing of the model. The individual model characteristics are given in table I. The areas given in figure 1 include wing and fin areas obtained by extending the leading and trailing edges to the center line. The center of gravity shown in figure 1 corresponds approximately to the design full-scale location. The centers of gravity of the tested models were located forward of this point as indicated in table I. Photographs of one of the models are shown in figures 2 to 4.

TESTS

The models were launched from a rail-type launcher (fig. 3) set at an elevation angle of approximately 60°. Flight-path velocity and atmospheric data were obtained by Doppler radar and radiosondes as in reference 1. Both models were equipped with two-channel nose-type telemeters that transmitted continuous signals of normal acceleration and angle of attack (reference 2) to two ground stations. A plot of Reynolds number against Mach number, shown in figure 5, indicates the scale of the tests.

REDUCTION OF DATA

Mach number was determined by the use of atmospheric data and flight-path velocity.

The values of normal acceleration for the deceleration phase of the flight were obtained from telemetered records (figs. 6 and 7) and reduced to coefficient form by the relationship

$$C_N = \frac{W}{qS_f} \frac{a_n}{g}$$

Since the angles of attack were small, normal force was considered lift. The telemetered records show one model to trim at positive angles of attack and the other to trim at negative angles of attack, but as the models were symmetrical the direction of trim is meaningless and was considered as positive to simplify subsequent figures. The rate of change of the lift coefficient with angle of attack was determined by graphically measuring the slope of a plot of C_N against α from data corrected for flight-path curvature and rate of pitch.

The periods of the short-period oscillations were determined from the time histories and used to evaluate static longitudinal stability by the following equation:

$$C_{m_\alpha} = -\frac{I_Y}{57.3qS_fC}\left[\frac{4\pi^2}{P^2} + \left(\frac{0.693}{T_{1/2}}\right)^2\right]$$

The aerodynamic centers for the flight conditions were found by subtracting the static margin, expressed as $\frac{dC_m}{dC_L} = \frac{C_{m_\alpha}}{C_{L_\alpha}}$, from the appropriate center-of-gravity location.

The time to damp to one-half amplitude was determined by first measuring the amplitude of two adjacent peaks from the trim line and applying the following equation:

$$T_{1/2} = \frac{0.693\ P}{2\ln\left(\frac{A_1}{A_2}\right)}$$

where A_1 and A_2 are the amplitude of peaks of either C_N or α.

The nondimensional damping factor was determined by the relationship

$$\left(C_{m_{\dot{\theta}d}}\frac{d}{2V} + C_{m_{\dot{\alpha}d}}\frac{d}{2V}\right) = \frac{-8I_Y}{57.3\rho VS_fd^2}\left(\frac{0.693}{T_{1/2}} - \frac{57.3C_{L_\alpha}\rho VS}{4\frac{W}{g}}\right)$$

[redacted]

A more complete analysis of the methods for the reduction of this type of data is found in reference 3. Also, a discussion of the accuracy of this type of investigation is found in reference 3.

The values of drag were obtained by the differentiation of the curve of Doppler flight-path velocity against time.

RESULTS AND DISCUSSION

Lift

The values of trim normal-force coefficient varied with Mach number and center-of-gravity location (fig. 8). Because of low stability near 0° angle of attack, slight constructional asymmetries caused the trim normal-force coefficients to be of appreciable values. With the center-of-gravity location at station 38.6 (model A), trim C_N increased from 0.5 at subsonic speeds to 1.2 at a Mach number of 1.02 and then gradually decreased to 0.5 at supersonic speeds. An erratic change in trim occurred between 0.93 and 0.96. With the center of gravity located at station 40.4 (model B), trim C_N varied from 1.0 at subsonic speeds to 3.0 at a Mach number of 0.975, decreased to approximately 1.6 at a Mach number of 1.35, and then gradually increased to 1.7 at a Mach number of 1.6. A slight change in trim occurred around a Mach number of 0.85.

Lift-curve slope varied with Mach number and C_N (fig. 9). For both low (model A) and high (model B) values of trim C_N, the lift-curve slope was at a maximum at a Mach number of approximately 1.25. At this Mach number, an increase in trim C_N from 0.65 to 1.65 was accompanied by an increase in C_{L_α} from 0.70 to 0.88. Below this Mach number, C_{L_α} fell off gradually to 0.55 (low C_N) and 0.65 (high C_N) at a Mach number of 0.8. These values agree favorably with low subsonic values of C_{L_α} from Langley Stability-Tunnel tests (reference 4). As the Mach number increased above 1.25, C_{L_α} decreased to values of 0.51 (low C_N) and 0.80 (high C_N) at a Mach number of 1.5, which are in fairly good agreement with data at a Mach number of 1.72 obtained at the Supersonic Wind Tunnels Laboratory, Aberdeen Proving Grounds, Md., (reference 5).

The increase of lift-curve slope with C_N or angle of attack probably is due to an increase in rear-wing efficiency as the wing moves into a weaker region of downwash.

[redacted]

Static Longitudinal Stability

Periods of the short-period oscillations (fig. 10) were used to obtain values of pitching-moment-curve slope (fig. 11) which in turn were used with lift-curve slope and center-of-gravity locations to determine aerodynamic center (fig. 12). Considering the center of gravity to be at the design location, the data for model A indicated that the static margin varied from 0.65 body diameter at a Mach number of 0.8 and a C_N of 0.5 to 0.1 body diameter at a Mach number of 1.0 and a C_N of 1.2, and then increased to 0.65 body diameter at a Mach number of 1.4 and a C_N of 0.5. The data from model B indicated that the static margin varied from 0.65 body diameter at a Mach number of 0.8 and a C_N of 1.0 to 1.0 body diameter at a Mach number of 1.02 and a C_N of 3.0 and then decreased to 0.65 body diameter at a Mach number of 1.5 and a C_N of 1.6.

Dynamic Longitudinal Stability

A qualitative evaluation of the dynamic stability of the two models can be made by an inspection of the short-period oscillations produced by the pulse rockets (figs. 6 and 7). The pulse rocket is thrusting in the first 0.12 second from the beginning of the disturbance so this part of the oscillation should be disregarded.

Both models appear to be dynamically stable in the supersonic range. The disturbance of model A (fig. 6) at 6.77 seconds (approx. a Mach number of 1) apparently produced an unstable oscillation before it damped out. Both the fact that the pulse rocket was thrusting during most of the unstable portion of the oscillation and the possibility of erratic trim changes at this Mach number forestall a conclusion of dynamic instability. The subsonic oscillation for this model was well damped.

The transonic oscillations of model B were well damped about a rapidly changing trim line. The subsonic oscillation was poorly damped for the first cycle but then decayed rapidly.

The variation of time to damp to one-half amplitude with Mach number under model flight conditions is presented in figure 13. The total damping factor (fig. 14) varied with normal-force coefficient and Mach number and was largest for both models at approximately a Mach number of 1.25. Except near a Mach number of 1.0 the damping factor was larger for model A. At a Mach number of 1.0 the damping factor was of about the same magnitude for both models. The equation for the total damping factor consists of two parts: a negative quantity containing $T_{1/2}$

and a positive quantity containing C_{L_α}. In general, the quantity containing $T_{1/2}$ was of approximately twice the magnitude of the quantity containing C_{L_α}.

Drag

The drag coefficient for the configuration increased with C_N and was largest in the transonic region (fig. 15).

CONCLUSIONS

A free-flight investigation of the static and dynamic longitudinal stability characteristics of $\frac{1}{3.7}$-scale rocket-powered models of the Bell MX-776A indicated the following conclusions:

1. With all control surfaces at 0° deflection the configuration was longitudinally stable when trimmed in free flight with the center of gravity located 1/4 and 1/2 body diameter ahead of the design location.

2. The variations of lift and pitching moment with angle of attack were not linear, both being at a minimum near 0° angle of attack. This nonlinearity was most pronounced in the transonic region.

3. The damping was at a maximum at a Mach number of 1.25.

Langley Aeronautical Laboratory
National Advisory Committee for Aeronautics
Langley Air Force Base, Va.

David H. Michal
Aeronautical Research Scientist

Approved:

Robert R. Gilruth
Chief of Pilotless Aircraft Research Division

GMF

[redacted]

REFERENCES

1. Michal, David H., and Mitcham, Grady L.: Preliminary Results of a Free-Flight Investigation of the Static Stability and Aileron Control Characteristics of $\frac{1}{6}$-Scale Models of the Bell MX-776. NACA RM SL9D21, U. S. Air Force, 1949.

2. Mitchell, Jesse L., and Peck, Robert F.: An NACA Vane-Type Angle-of-Attack Indicator for Use at Subsonic and Supersonic Speeds. NACA RM L9F28a, 1949.

3. Gillis, Clarence L., Peck, Robert F., and Vitale, A. James: Preliminary Results from a Free-Flight Investigation at Transonic and Supersonic Speeds of the Longitudinal Stability and Control Characteristics of an Airplane Configuration with a Thin Straight Wing of Aspect Ratio 3. NACA RM L9K25a, 1950.

4. Queijo, M. J., and Michael, W. H., Jr.: Wind-Tunnel Investigation of the Low-Speed Static Stability and Control Characteristics of a Model of Bell MX-776. NACA RM SL9G08, U. S. Air Force, 1949.

5. Speth, Robert F.: Results of Shrike (MX 776A) Supersonic Wind Tunnel Tests at M = 1.72. Rep. No. 59-980-002, Bell Aircraft Corp., Aug. 19, 1949.

TABLE I

MODEL CHARACTERISTICS DURING THE UNPOWERED PORTION OF THE FLIGHT

[Station numbers correspond to the distance in inches from the point of the nose]

Model	Weight (lb)	Center-of-gravity location, station	Moment of inertia about pitch axis (slug-ft^2)
A	53.3	38.6	5.32
B	48.4	40.4	4.77

NACA

[redacted]

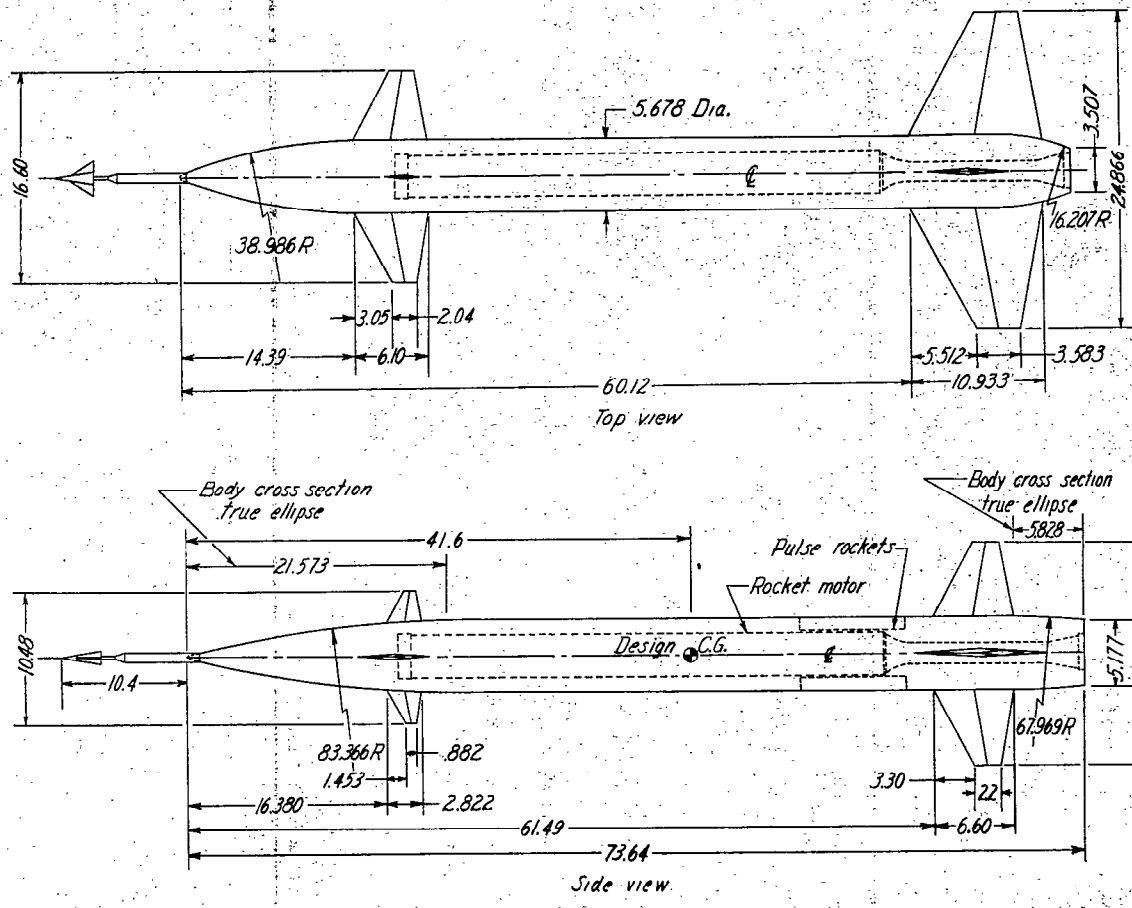

	Included area	Aspect ratio
Aft hor. wing	1.422 ft^2	3.02
Aft vert. fin	0.664 ft^2	3.18
Forward hor. wing	0.592 ft^2	3.24
Forward vert. fin	0.204 ft^2	3.73

All airfoils are of a symmetrical double wedge section of 0.05 thickness ratio

All dimensions are in inches

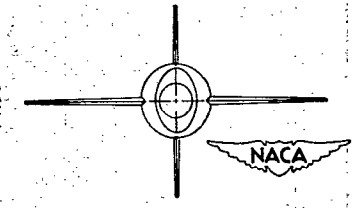

Rear view

Figure 1.- General arrangement of $\frac{1}{3.7}$-scale Bell MX-776A rocket-powered flight model.

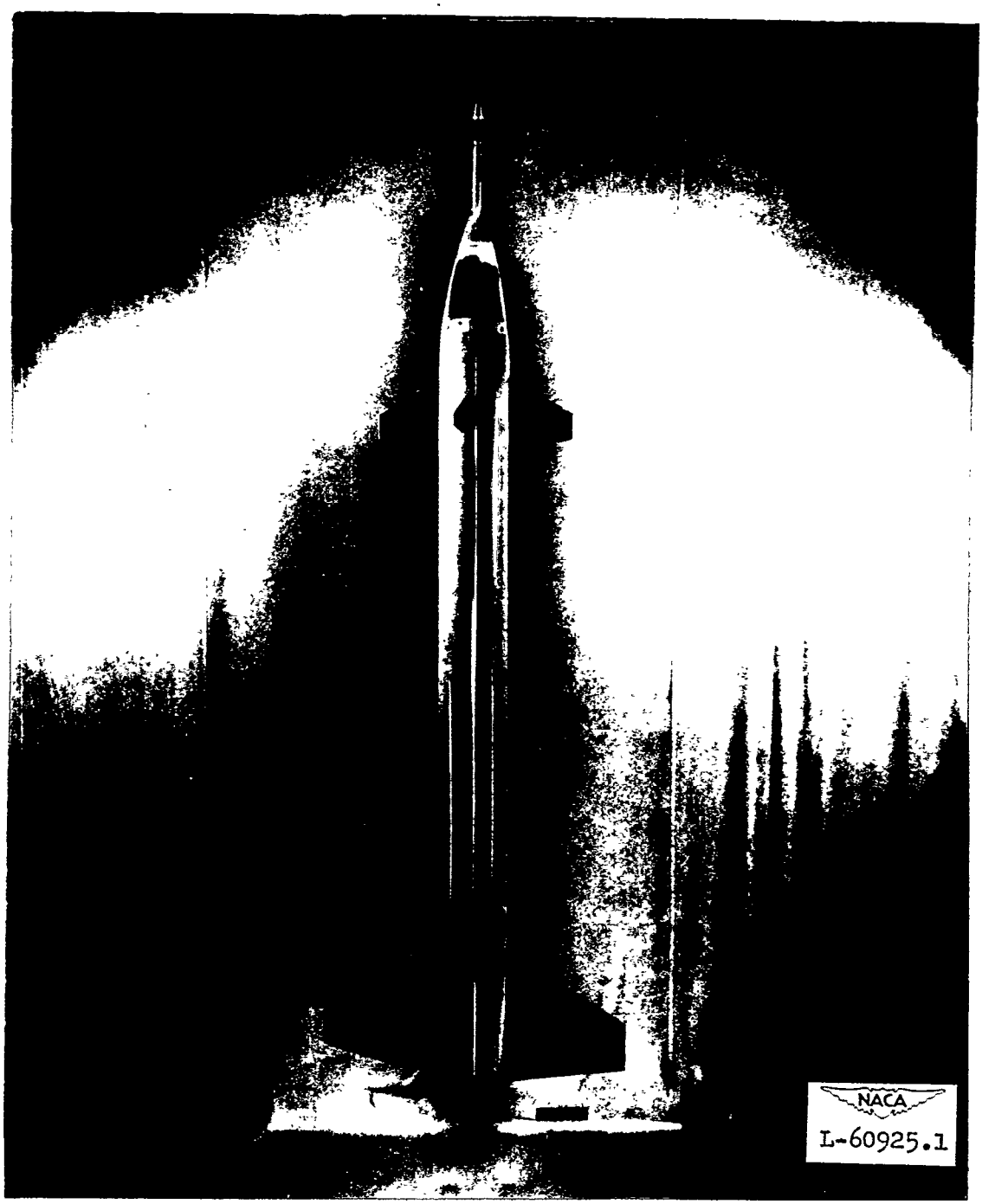

Figure 2.- Bell MX-776A rocket-powered flight test model.

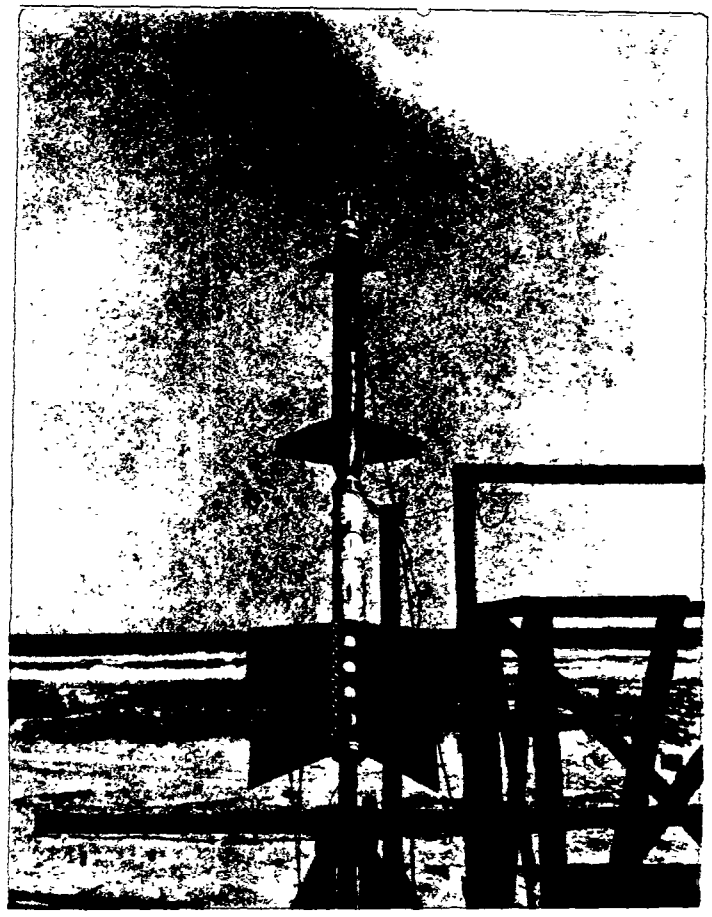

NACA

L-61809

Figure 3.- Model and booster on launcher.

Figure 4.- Angle-of-attack indicator and telemeter section.

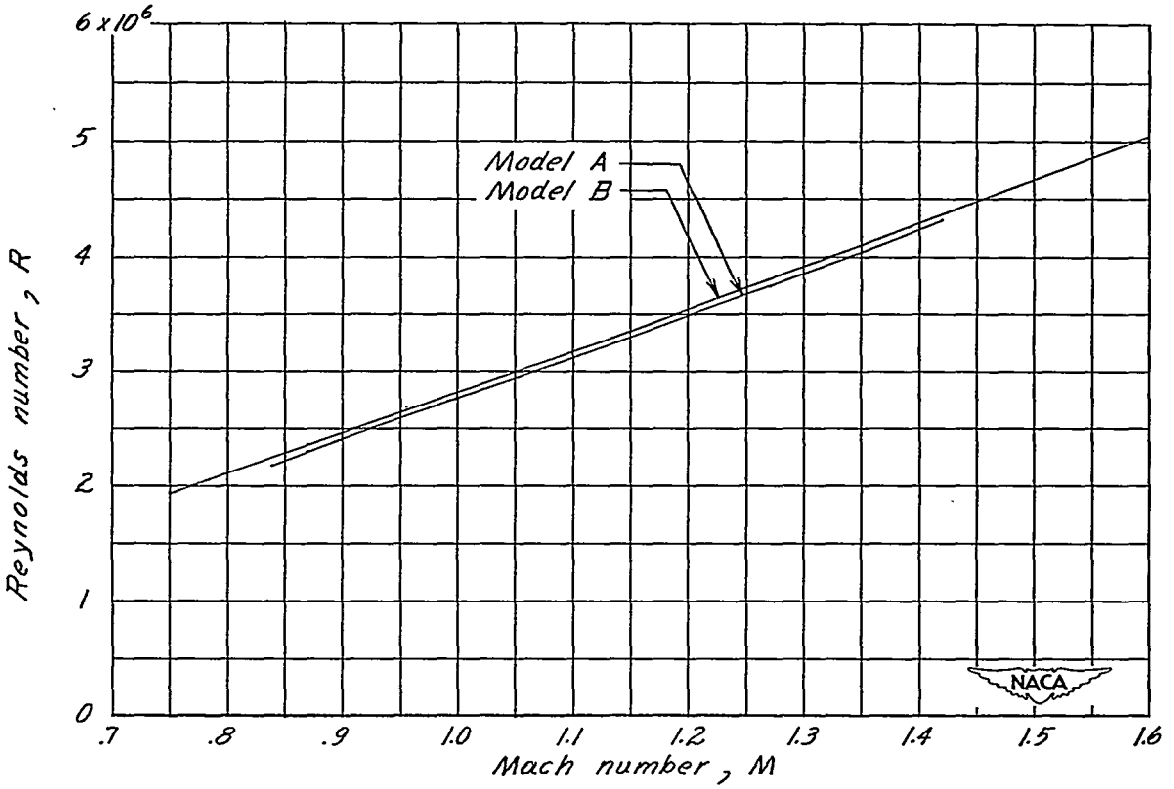

Figure 5.- Variation of Reynolds number with Mach number.

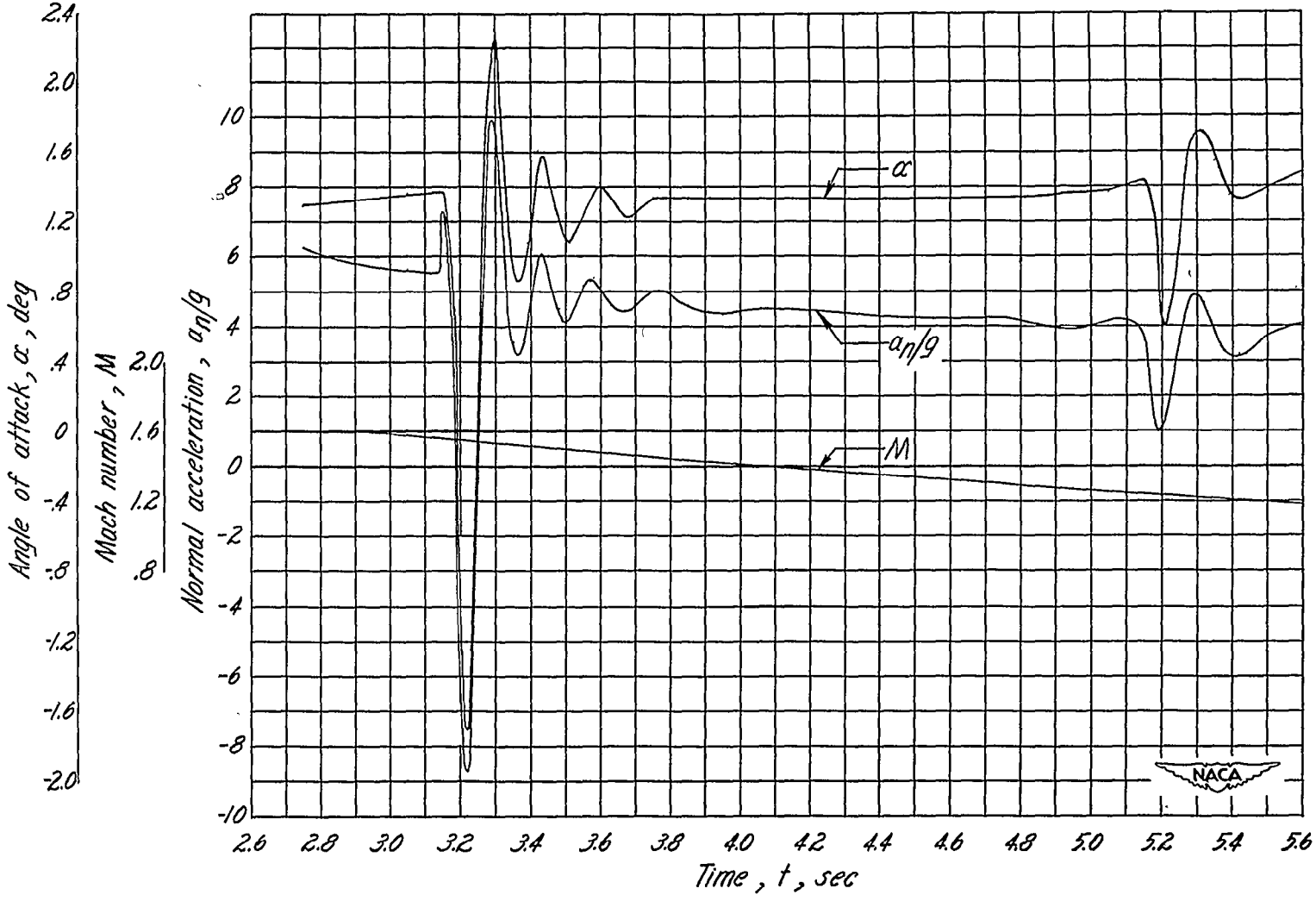

Figure 6.- Time history of flight of the model with center of gravity located at station 38.6. Model A.

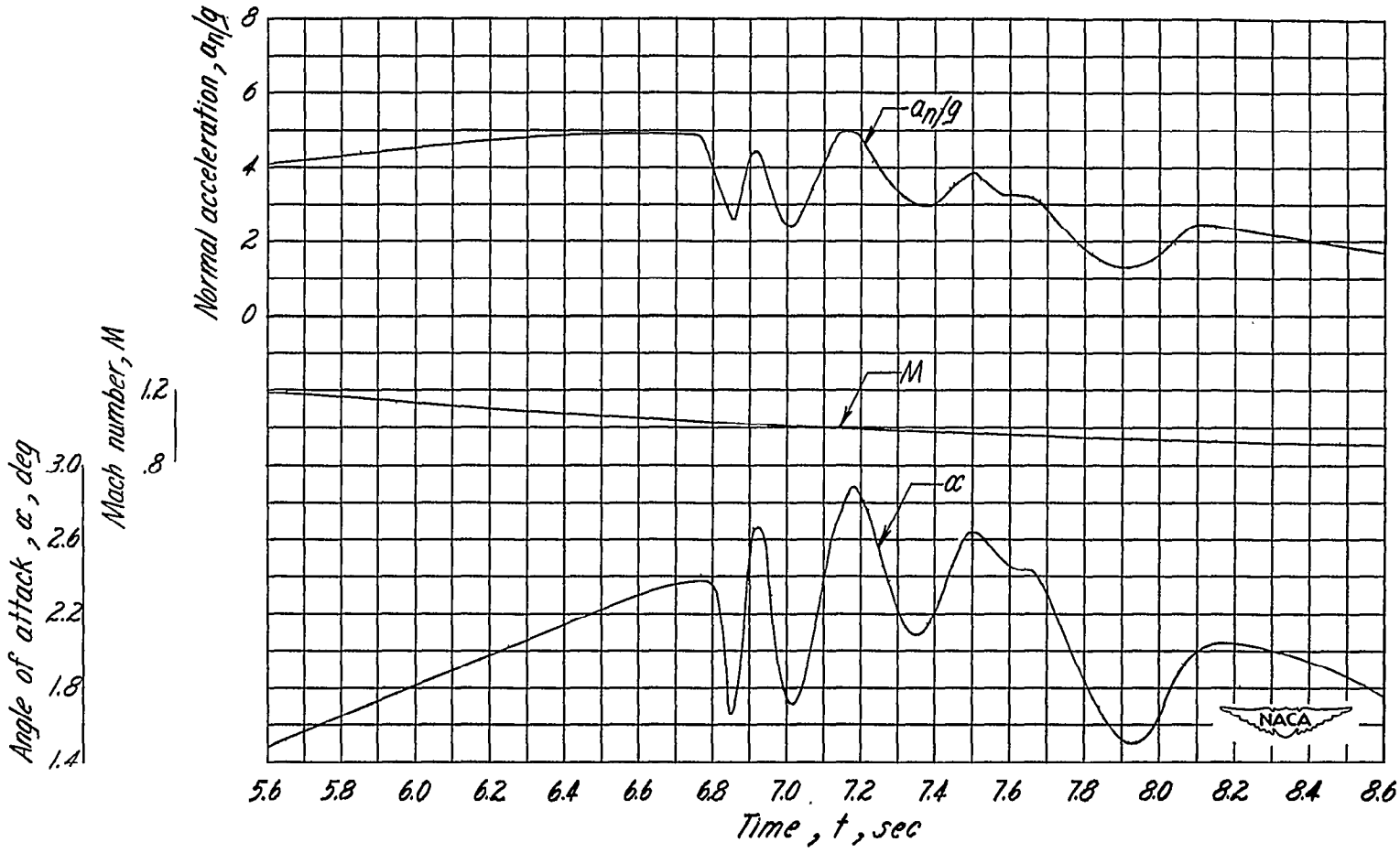

Figure 6.- Continued.

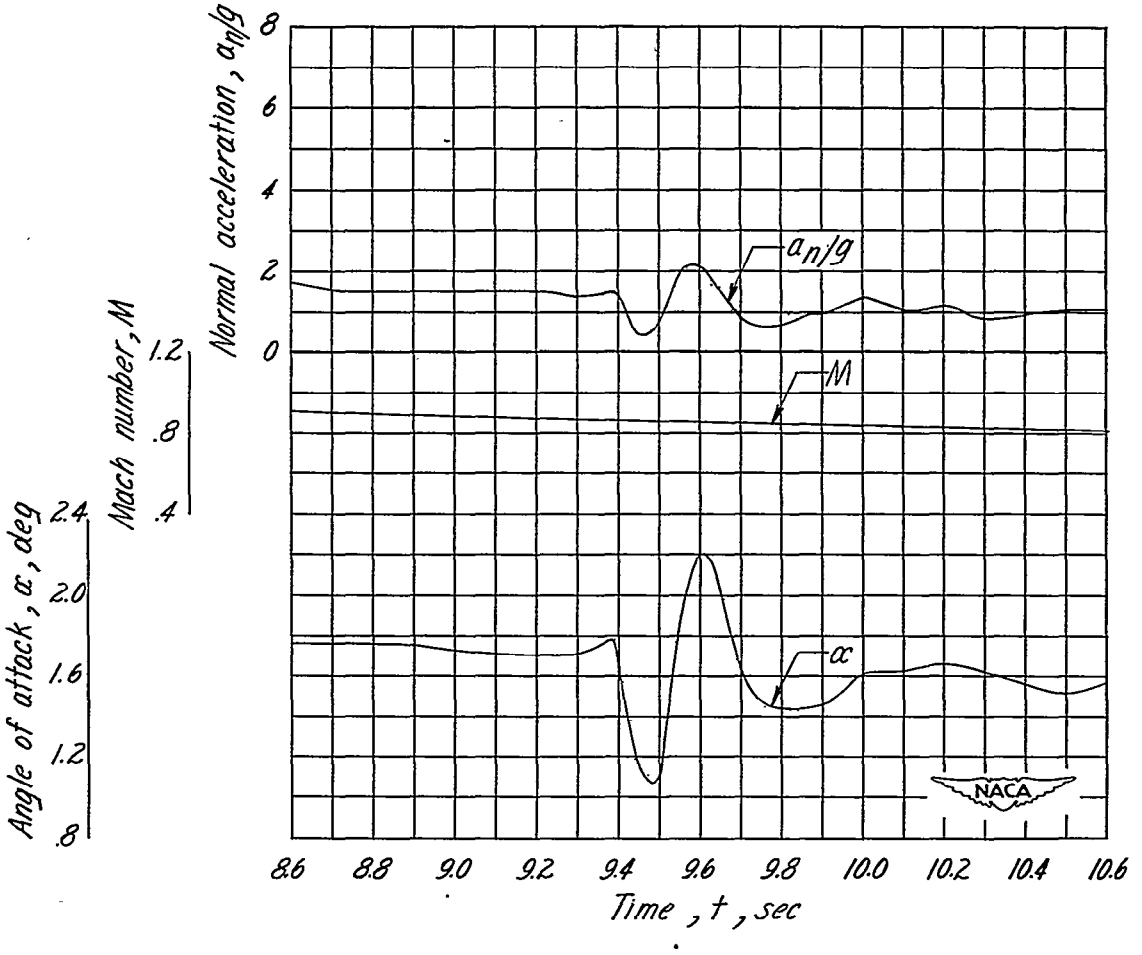

Figure 6.- Concluded.

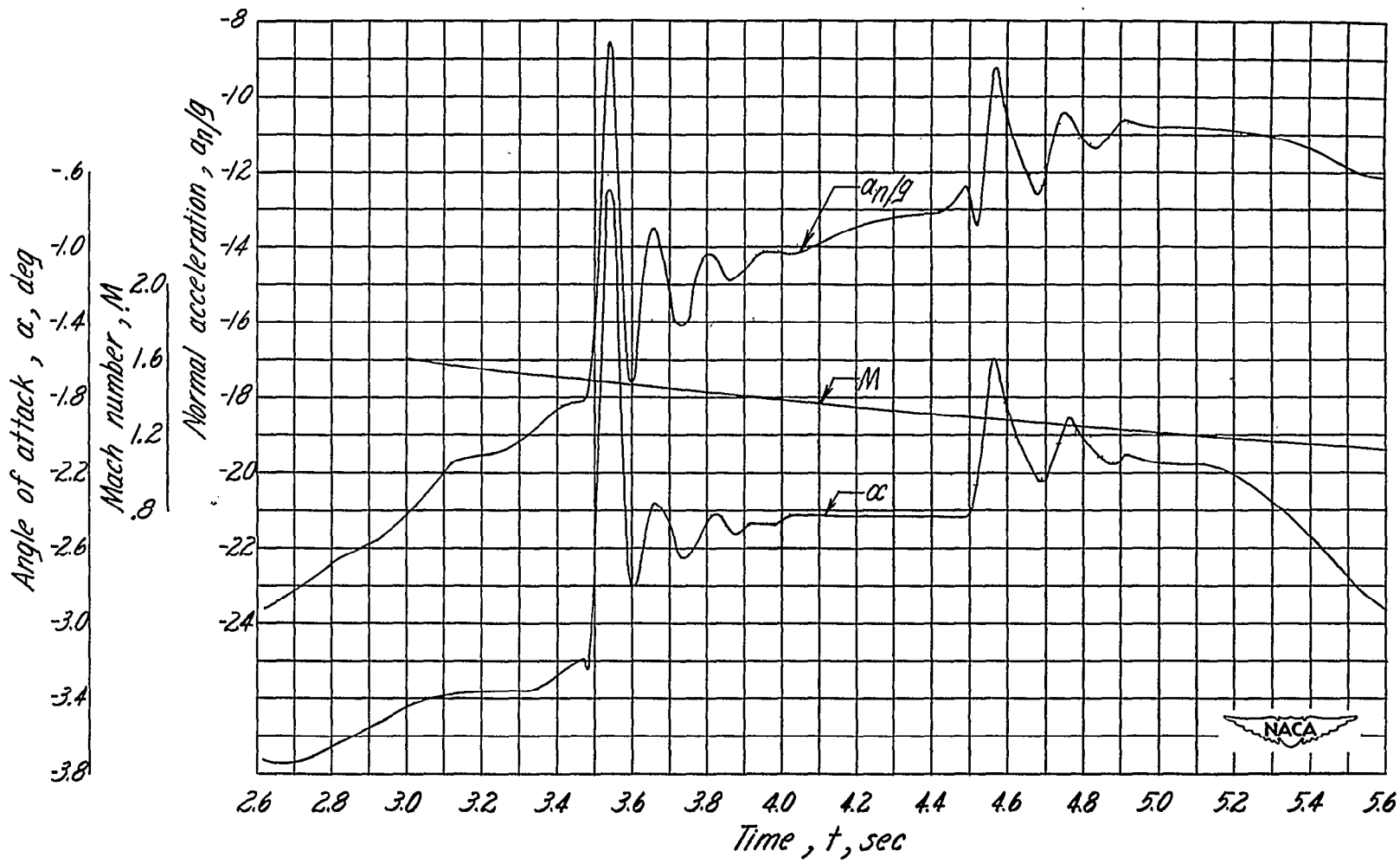

Figure 7.- Time history of flight of the model with center of gravity located at station 40.4. Model B.

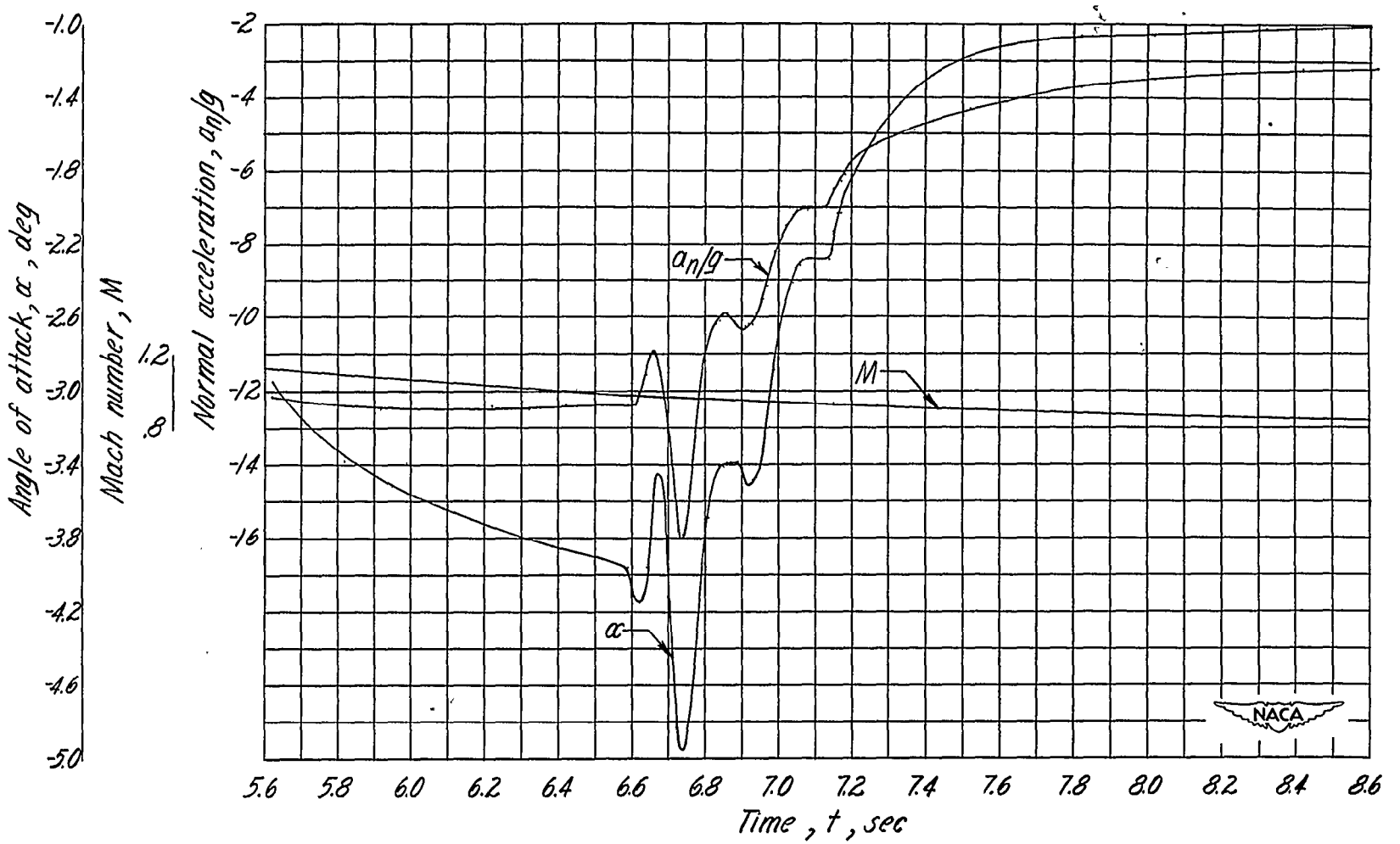

Figure 7.- Continued.

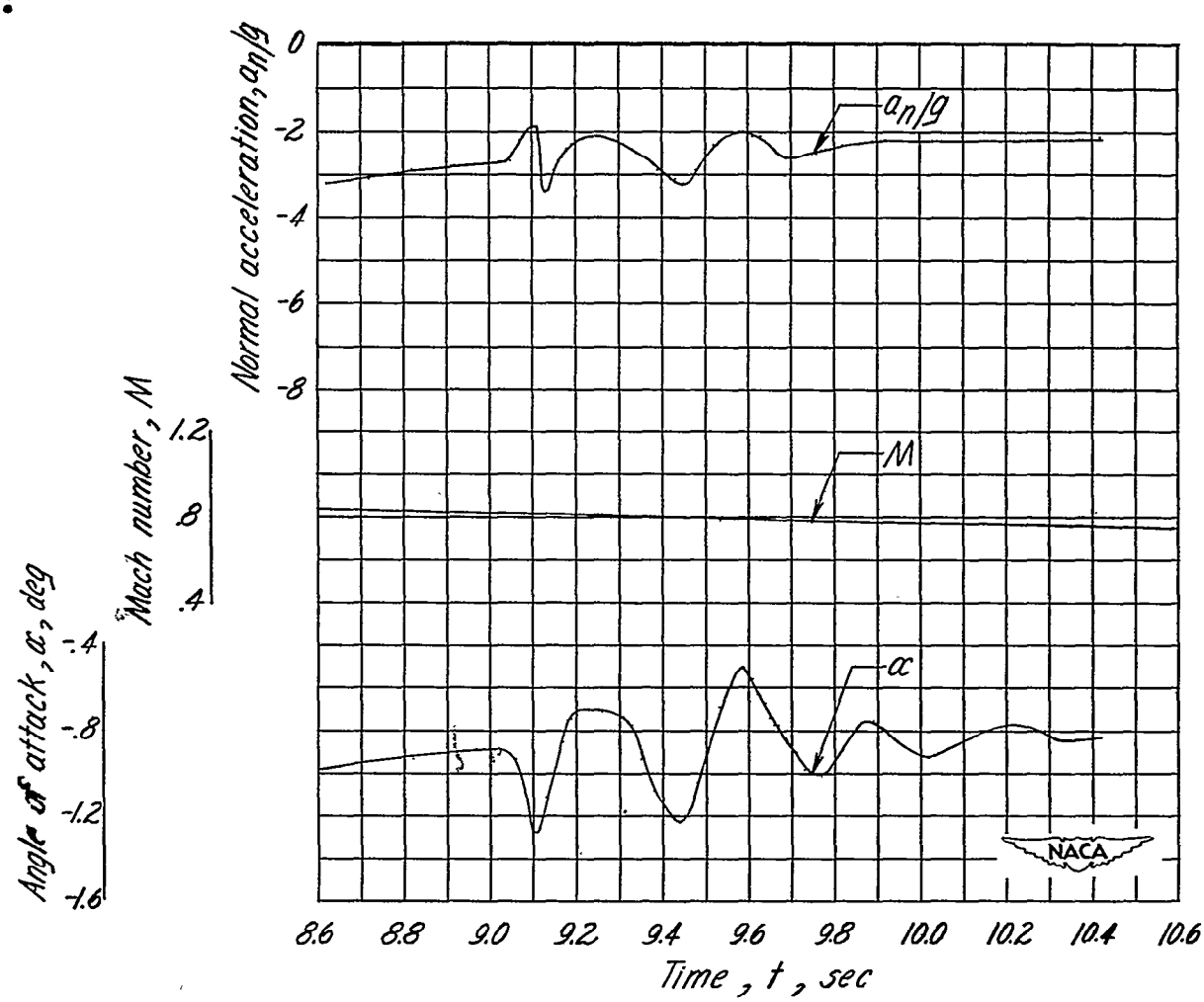

Figure 7.- Concluded.

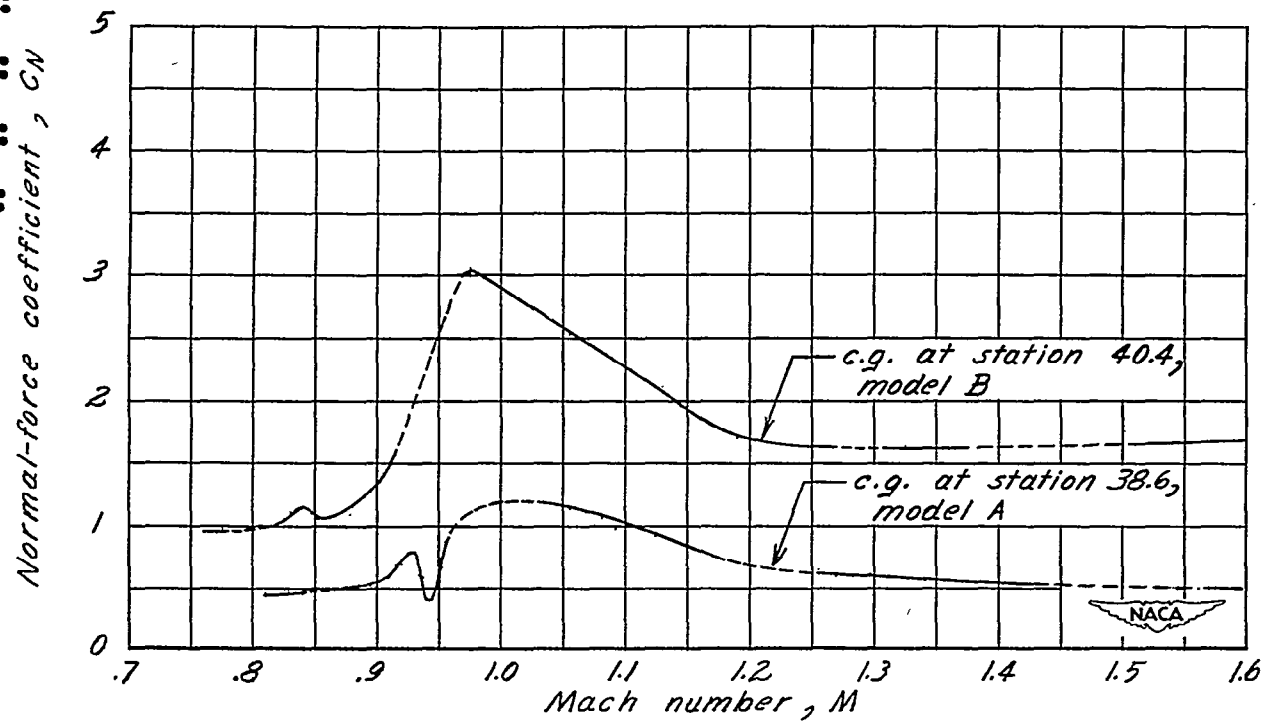

Figure 8.- Variation of trim normal-force coefficients with Mach number.

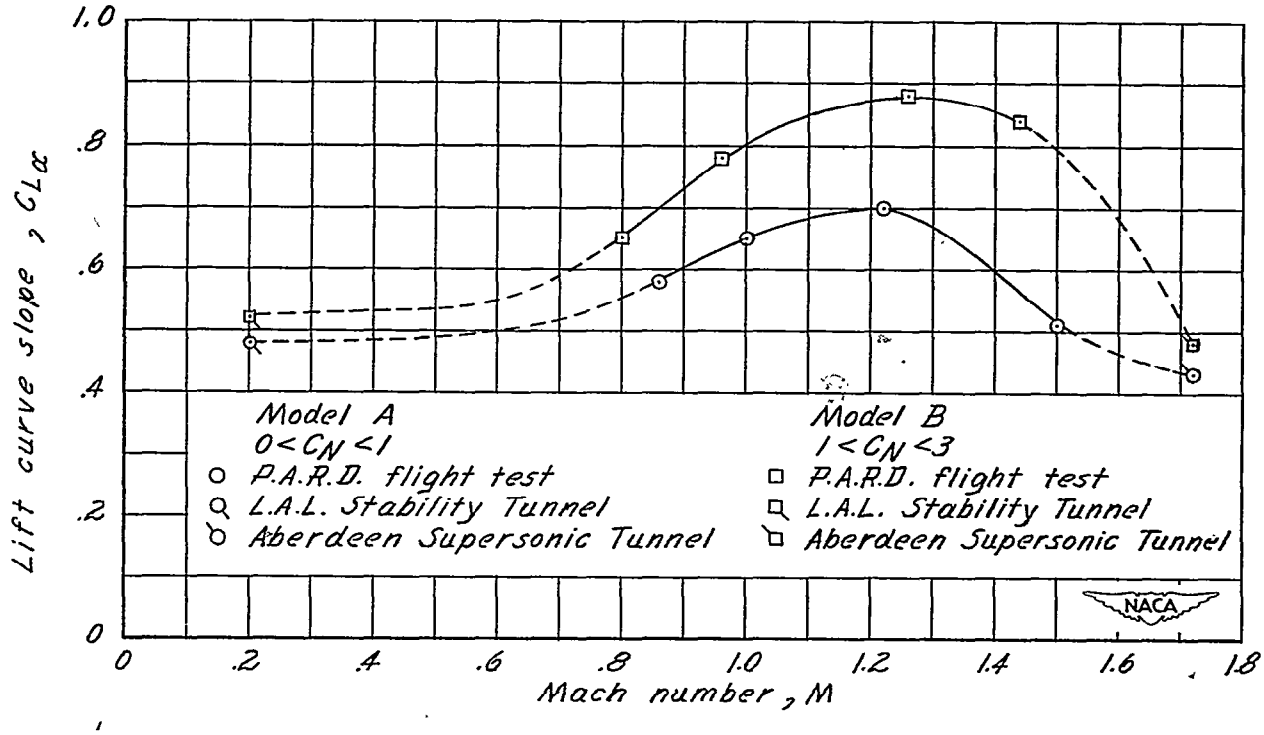

Figure 9.- Variation of lift-curve slope with Mach number.

[redacted]

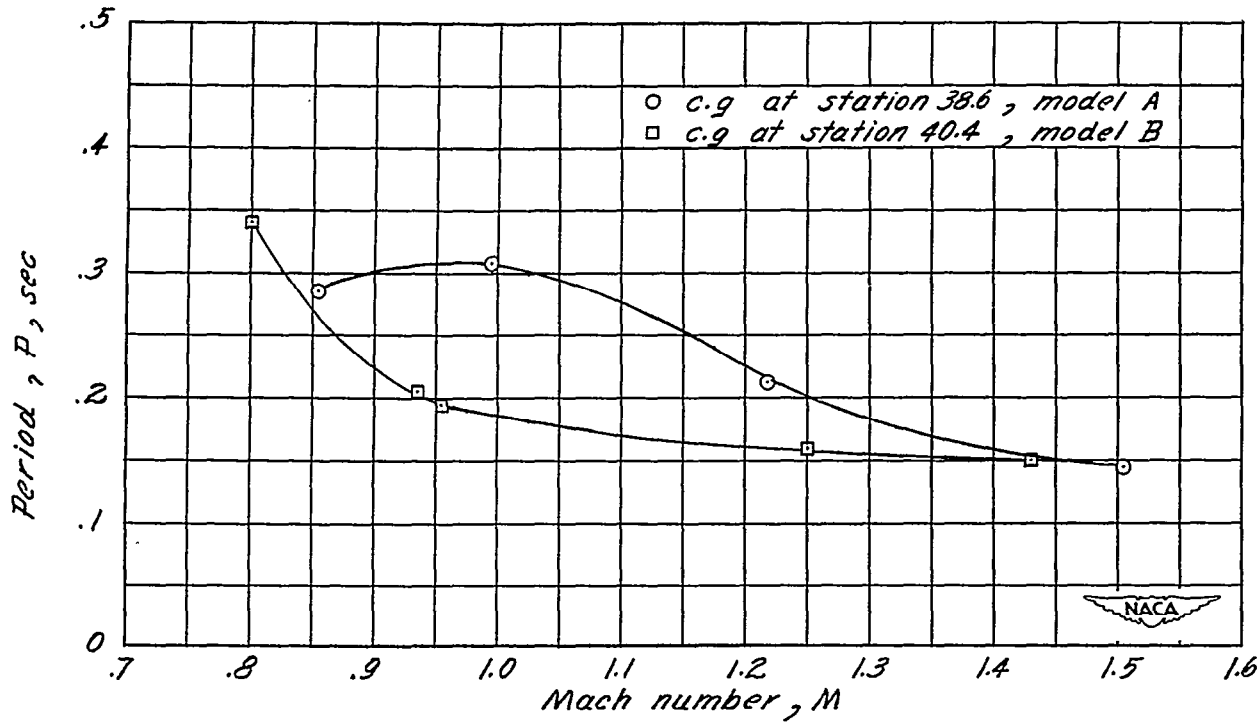

Figure 10.- Period of short-period oscillations as a function of Mach number.

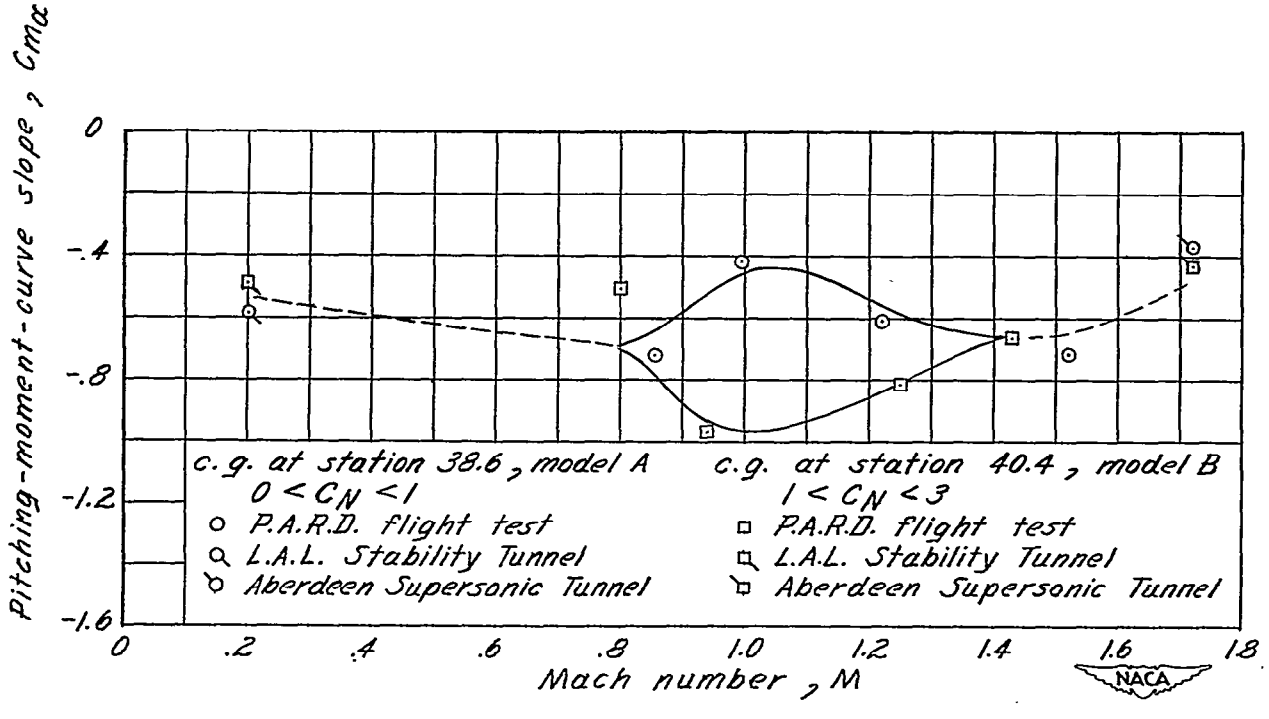

Figure 11.- Variation of pitching-moment-curve slope with Mach number.

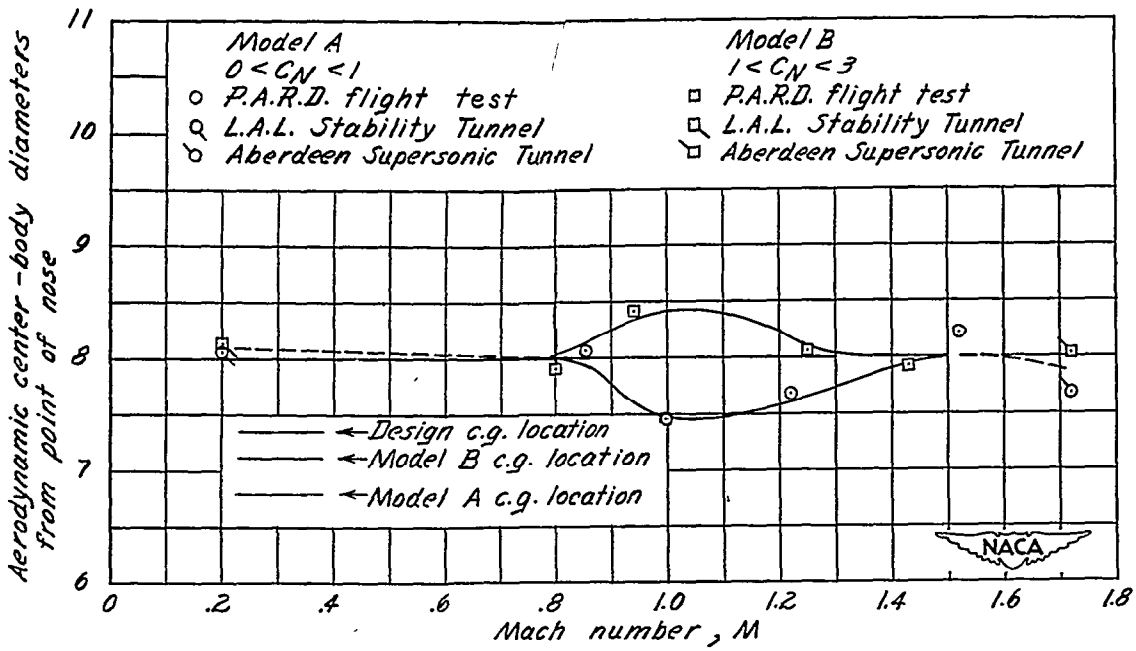

Figure 12.- Variation of aerodynamic center with Mach number.

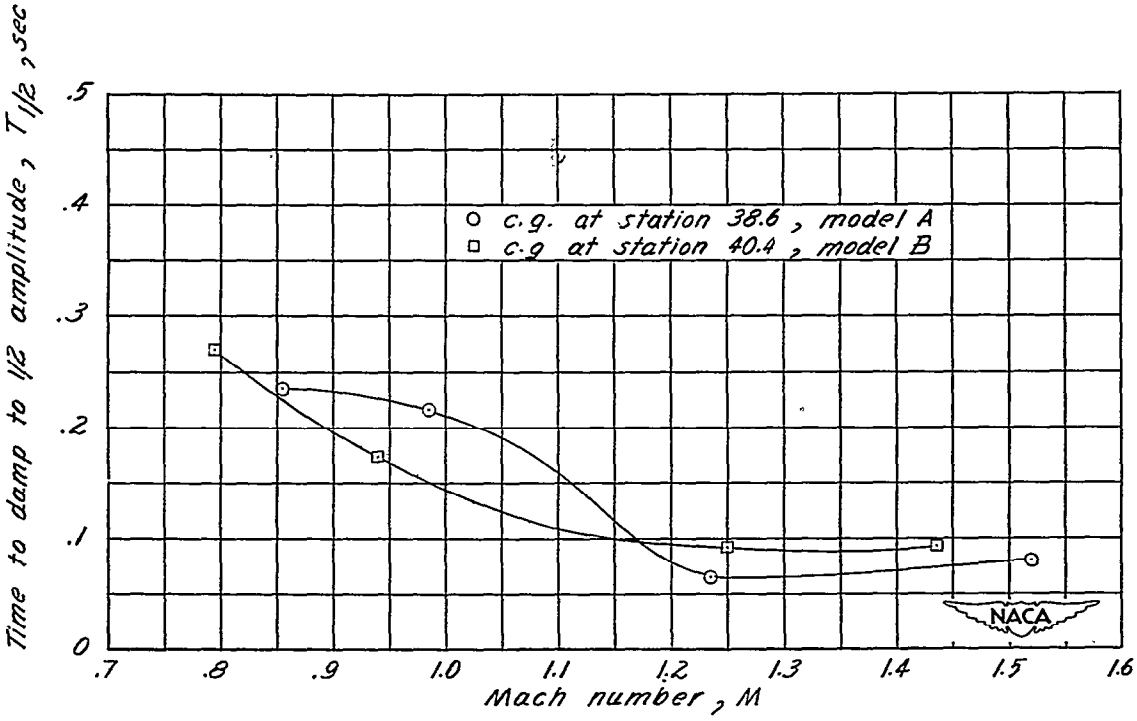

Figure 13.- Variation of the time for the short-period oscillations to damp to one-half amplitude with Mach number under model flight conditions.

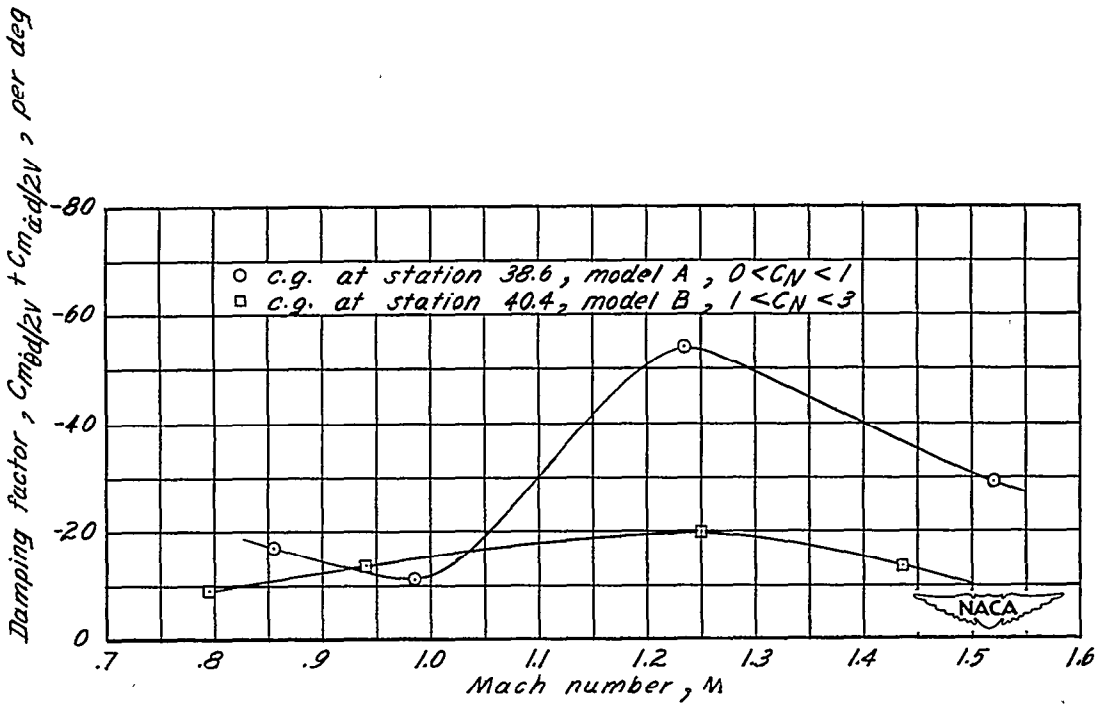

Figure 14.- Variation of damping factor with Mach number.

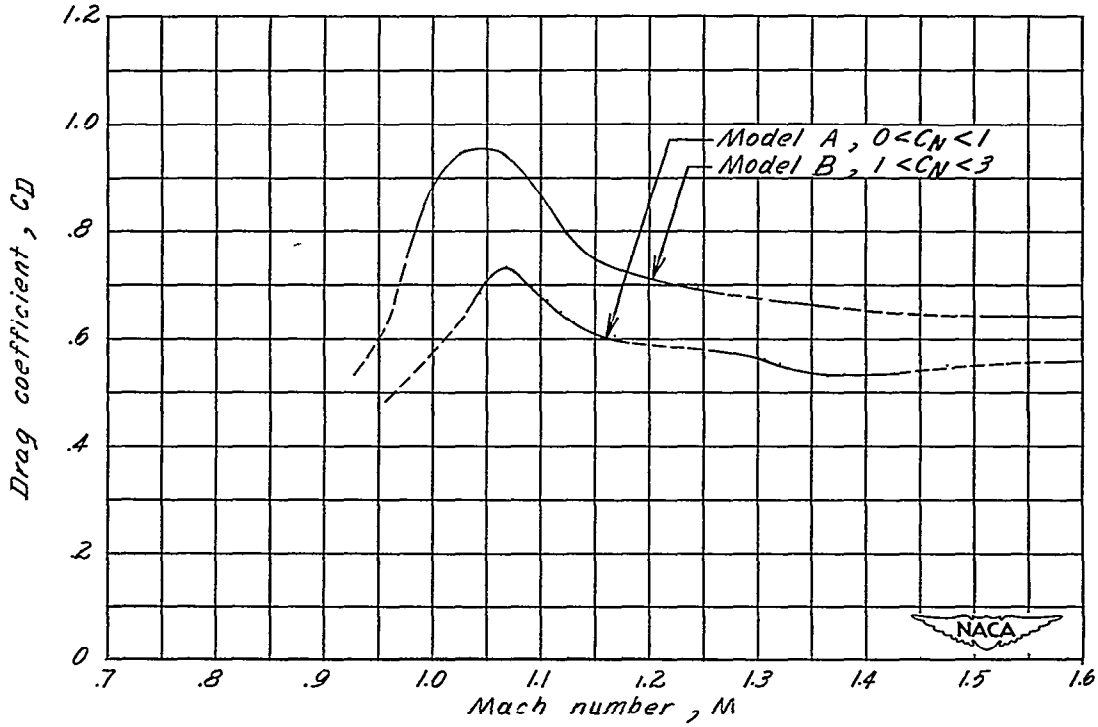

Figure 15.- Variation of trim drag coefficients with Mach number.